Electronic Supplementary Material (ESI) for Journal of Materials Chemistry A.

Supporting Information

for

Selective host-guest interactions in metal-organic frameworks via multiple hydrogen bond donor-acceptor recognition sites

Thomas Wittmann[†], Carsten B. L. Tschense[†], Lisa Zappe[†], Charlotte Koschnick[#], Renee Siegel[†], Robert Stäglich[†], Bettina V. Lotsch[#], Jürgen Senker[†,*]

[†] Department of Inorganic Chemistry III and Northern Bavarian NMR Centre (NBNC), University of Bayreuth, Universitätsstraße 30, 95440 Bayreuth (Germany)

[#] Max Planck Institute for Solid State Research, Heisenbergstr. 1, 70569 Stuttgart, Germany and Department of Chemistry, University of Munich (LMU), Butenandtstr. 5-13, 81377 Munich, Germany

[*] juergen.senker@uni-bayreuth.de

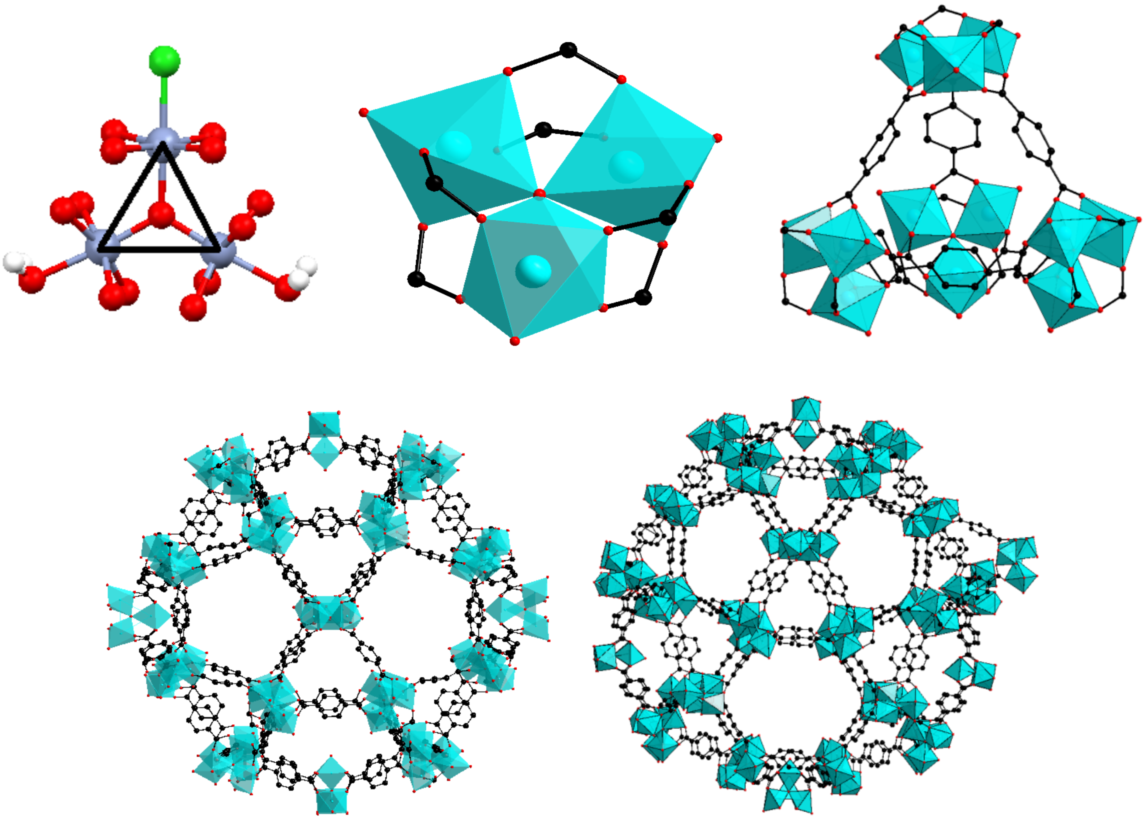

Figure S1: Structure of MIL-101. The metal ions in MIL-101 are arranged to form a equilateral triangle centred with a μ_3-oxygen atom (top left). The metal ions are octahedrally coordinated with four oxygen atoms from the terephthalate linkers, one corner sharing μ_3 oxygen and terminal position. Two of the three terminal positions are occupied by water molecules and one by chloride ions (top middle). The two water ligands can be exchanged by other coordinating species.[1–3] The inorganic building units (IBUs) are connected by terephthalate ligands to form a supertetrahedron with an inner diameter of 0.7 nm (top right). The supertetrahedra are in turn connected to form mesoporous cages with internal diameters of 2.5 nm (bottom left) and 3.0 nm (bottom right), which are accessible and interconnecting through pentagonal and hexagonal windows with diameters of 1.2 nm and 1.6 nm, respectively.

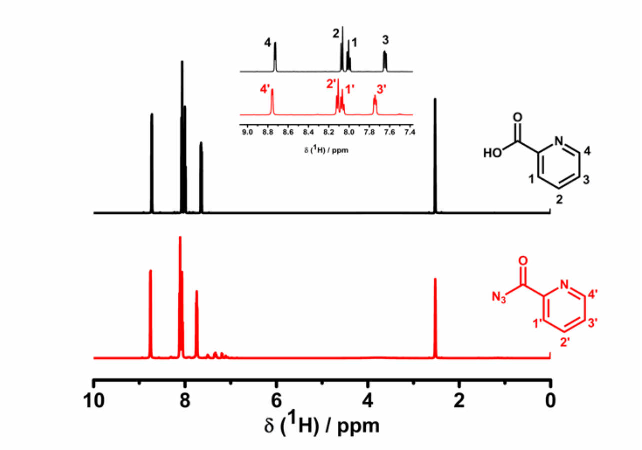

Figure S2: ^{1}H NMR spectra of 2-picolinic acid (top) and 2-pyridyl acyl azide in DMSO-d6 (bottom).

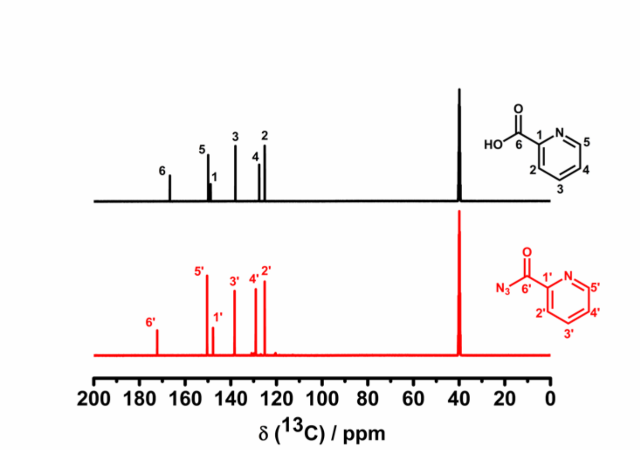

Figure S3: ^{13}C NMR spectra of 2-picolinic acid (top) and 2-pyridyl acyl azide in DMSO-d6 (bottom).

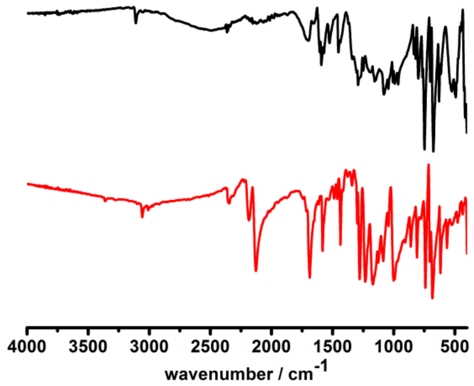

Figure S4: ATR-IR spectra of 2-picolinic acid (top) and 2-pyridyl acyl azide (bottom). The strong band 2130 cm^{-1} is attributed to the asymmetric stretching vibration of the azide group (bottom).

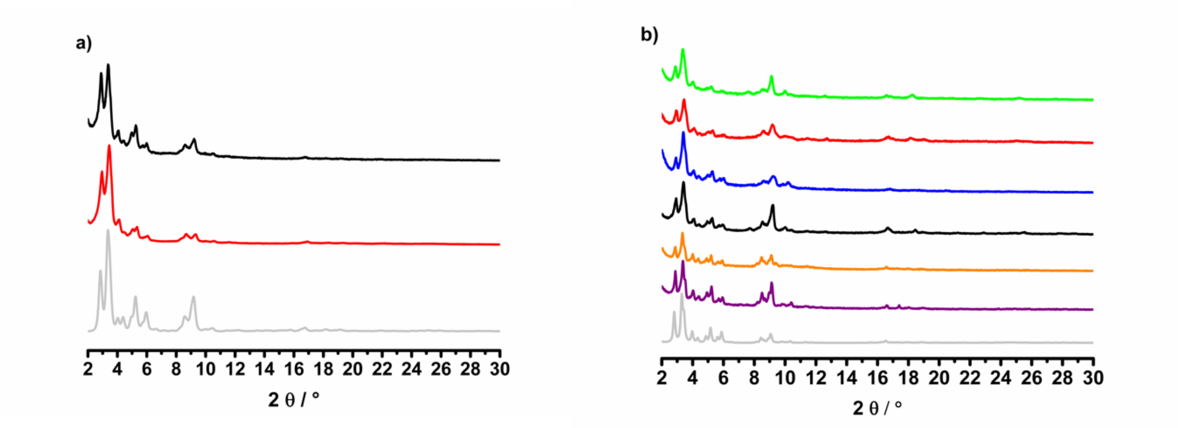

Figure S5: PXRD patterns of a) Al-MIL-101-NH_2 (black), Al-MIL-101-URPy (red) and the simulated pattern of Al-MIL-101 (grey) and of b) DEA-Cr-MIL-101-URPy (green), H_2O-Cr-MIL-101-URPy (red), DEA-Cr-MIL-101-NH_2 (blue), H_2O-Cr-MIL-101-NH_2 (black), DEA-Cr-MIL-101-H (orange), H_2O-Cr-MIL-101-H (violet) and the simulated pattern (grey) obtained from structure data.[4]

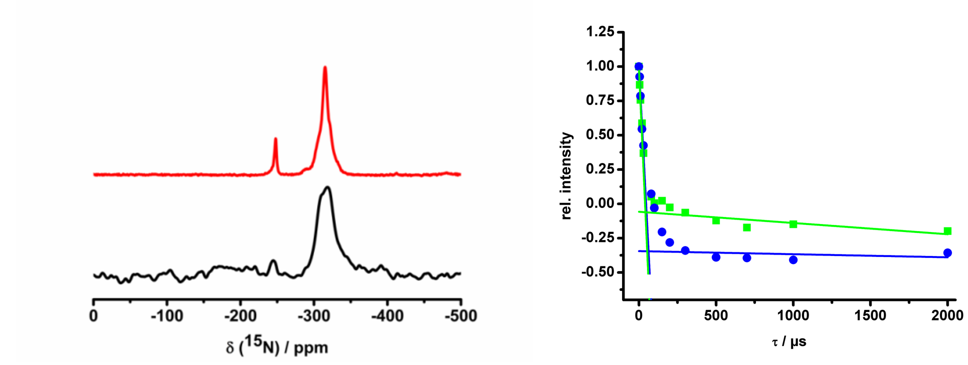

Figure S6: a) ^{15}N CP MAS NMR spectrum of Al-MIL-101-NH_2 (black line) and ^{15}N single pulse (SP) NMR spectrum of Al-MIL-101-NH_2 with 98% abundance of ^{15}N (red line). Both spectra show two signals one at -247 and one at -316 ppm. Based on the SP excitation the intensity ratio was estimated to 5:95.

b) Normalized signal intensities as a function of the inversion time for the signal at -247 ppm (green curve) and for the signal at -316 ppm (blue curve) of the solid-state ^{15}N MAS CPPI spectra of Al-MIL-101-NH_2. The transition points between the fast decaying region (0-200 µs) and the region with the slow decay (300 – 2000 µs) were extrapolated by fitting the trend within both regions with straight lines. The relative intensity at the transition point for a CPPI experiment represents the number of covalently bonded protons attached to one nitrogen atom. The turnover for the signal at -247 ppm occurs at zero while the one for the resonance at -316 ppm takes place at -0.35. The signal at -247 ppm is thus assigned to NH groups, which most probably arise due to a reaction of DMF with the aromatic amino function resulting in NHCHO pending groups. According to the low intensity of the ^{15}N SP NMR spectrum (Figure S6 a) the amount of such units within the final product is below 5%. For the signal at -316 ppm, we observed a turnover typical for NH_2 units and is thus assigned to the aromatic amino function.

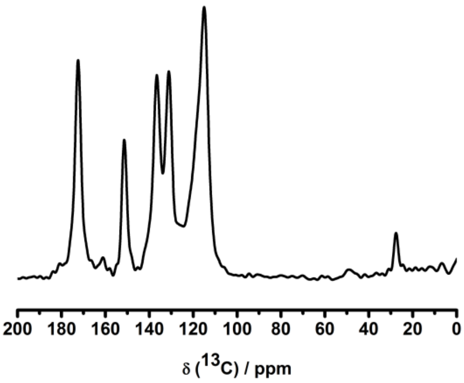

Figure S7: ^{13}C CP MAS spectrum of Al-MIL-101-NH_2 with 98% abundance of ^{15}N.

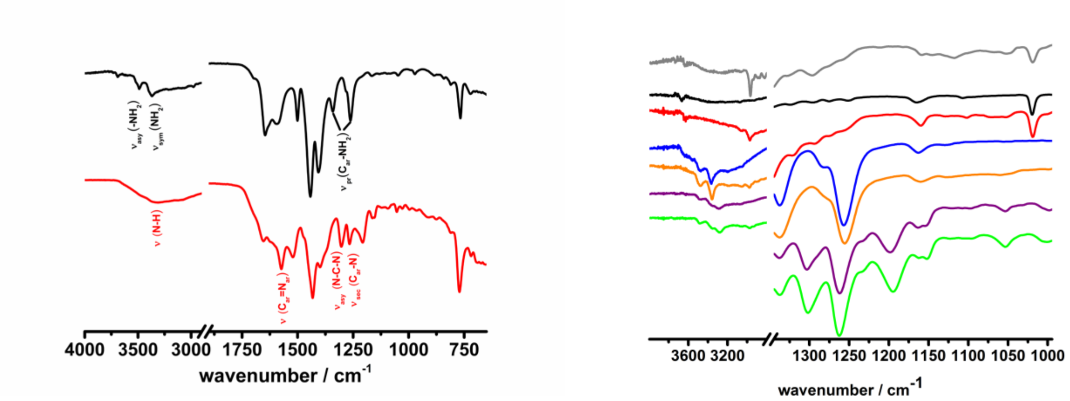

Figure S8: a) ATR-IR spectra of Al-AMIL-101-NH_2 (black line) and Al-MIL-101-URPy (red line); b) ATR-FTIR-spectra from bottom to top: DEA-Cr-MIL-101-URPy (green line), H_2O-Cr-MIL-101-URPy (violet line), DEA-Cr-MIL-101-NH_2 (orange line), H_2O-Cr-MIL-101-NH_2 (blue line), DEA-Cr-MIL-101-H (red line), H_2O-Cr-MIL-101-H (black line) and H_2O-Cr-MIL-101-H (grey line) soaked in diethylamine to evaluate the aliphatic and C-N IR vibrations of non-coordinated diethylamine (grey line). The incorporation of DEA is indicated by the small IR blueshifts of 9 cm^{-1} and 7 cm^{-1} for the aliphatic methylene C-H and C-N stretching vibration bands of coordinated DEA compared to the free ligand (2975 cm^{-1} vs. 2966 cm^{-1} and 1058 cm^{-1} vs. 1051 cm^{-1}, Figure S9b) are in line with the results for other alkyl amines.[2,3,5] In the case of the URPy framework the C-N stretching vibration of DEA is overlaid by the aromatic C-H stretching vibration band at 1053 cm^{-1} of 2-monosubstituted pyridines.[6]

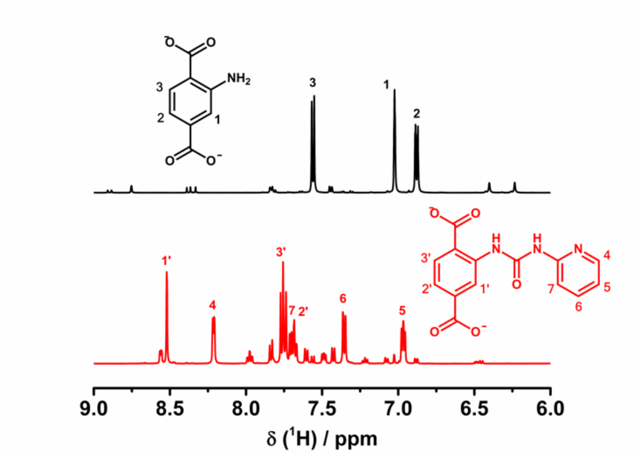

Figure S9: ^1H NMR spectra of Al-MIL-101-NH_2 (top) and Al-MIL-101-URPy (bottom) after digestion in 5 wt% of CsF in DMSO-d6/D_2O (5:1) together with the respective signal assignments. The yield of PSM was determined by comparing the integrated areas of the aromatic resonances 1' with 1 of Al-MIL-101-URPy (bottom), representing the ortho-protons of the unmodified and modified linkers relative to the amino and pyridyl urea group, respectively.

Table S1: Al, Cr, C, H, N weight contents and the metal to chloride ratio of Al-MIL-101-NH_2 and Al-MIL-101-URPy, H_2O-Cr-MIL-101-H, DEA-Cr-MIL-101-H, H_2O-Cr-MIL-101-NH_2, DEA-Cr-MIL-101-NH_2, H_2O-Cr-MIL-101-URPy and DEA-Cr-MIL-101-URPy.

	H exp	H theo	C exp	C theo	N exp	N theo	Al/Cr exp	Al/Cr theo	Al/Cr:Cl
Al-MIL-101-NH_2 $Al_3O(H_2O)_2Cl(bdc)_3$	2.79	2.72	42.05	40.88	5.89	5.96	10.87	11.47	3.05:1
Al-MIL-101-URPy **(90% URPy)** $Al_3O(H_2O)_2Cl(bdc\text{-}NH_2)_{0.3}(bdc\text{-}URPy)_{2.7}$	3.12	2.93	46.63	46.99	10.97	11.51	7.36	7.78	3.05:1
H_2O-Cr-MIL-101-H $Cr_3O(H_2O)_2(OH)_{0.8}(NO_3)_{0.2}(bdc)_3$	2.69	2.34	40.09	39.68	0.38	0.38	22.06	21.47	---
DEA-Cr-MIL-101-H **(88% DEA)** $Cr_3O(H_2O)_{0.5}(DEA)_{1.76}\text{-}(OH)_{0.8}(NO_3)_{0.2}\ (bdc)_3$	3.95	4.10	43.85	44.89	3.48	3.22	17.80	18.72	---
H_2O-Cr-MIL-101-NH_2 $Cr_3O(H_2O)_{2.1}Cl_{0.9}(bdc\text{-}NH_2)_3$	2.44	2.49	37.22	37.01	5.32	5.39	18.96	20.02	3.35:1
DEA-Cr-MIL-101-NH_2 **(75% DEA)** $Cr_3O(H_2O)_{0.85}(DEA)_{1.5}Cl_{0.95}(bdc\text{-}NH_2)_3$	3.73	3.94	41.41	41.56	6.57	6.96	18.71	18.10	3.08:1
H_2O-Cr-MIL-101-URPy **(90% URPy)** $Cr_3O(H_2O)_{2.04}Cl_{0.96}(bdc\text{-}NH_2)_{0.3}(bdc\text{-}URPy)_{2.7}$	2.81	2.71	43.70	43.42	11.16	10.45	13.65	14.33	3.12:1
DEA-Cr-MIL-101-URPy **(90% URPy, 60% DEA)** $Cr_3O(H_2O)_{1.05}(DEA)_{1.2}Cl_{0.97}(bdc\text{-}NH_2)_{0.3}(bdc\text{-}URPy)_{2.7}$	3.76	3.63	46.28	45.89	10.97	11.17	13.60	13.49	3.04:1

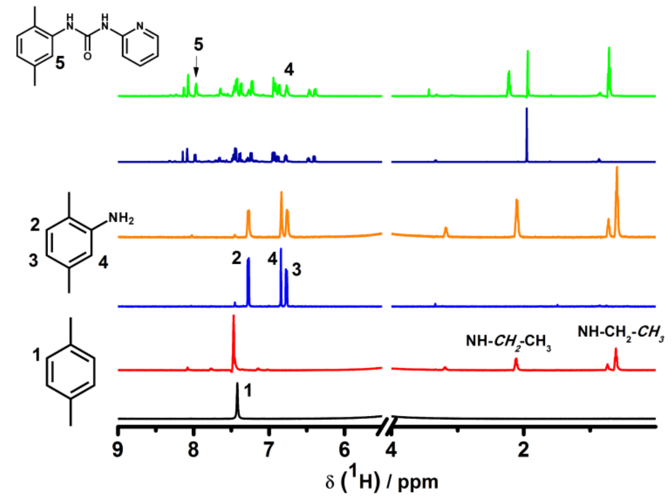

Figure S10: Solution ^{1}H NMR spectra from bottom to top: H_2O-Cr-MIL-101-H (black line), DEA-Cr-MIL-101-H (red line), H_2O-Cr-MIL-101-NH_2 (blue line), DEA-Cr-MIL-101-NH_2 (orange line), H_2O-Cr-MIL-101-URPy (violet line), DEA-Cr-MIL-101-URPy (green line). Due to degradation of the urea pyridine unit in the more basic dissolution medium for the Cr-compounds, the intensities of the 1H NMR spectra for H_2O-Cr-MIL-101-URPy and DEA-Cr-MIL-101-URPy underestimate the degree of the PSM. We thus rely exclusively on the results of the elemental analysis and AAS for quantification for these two cases.

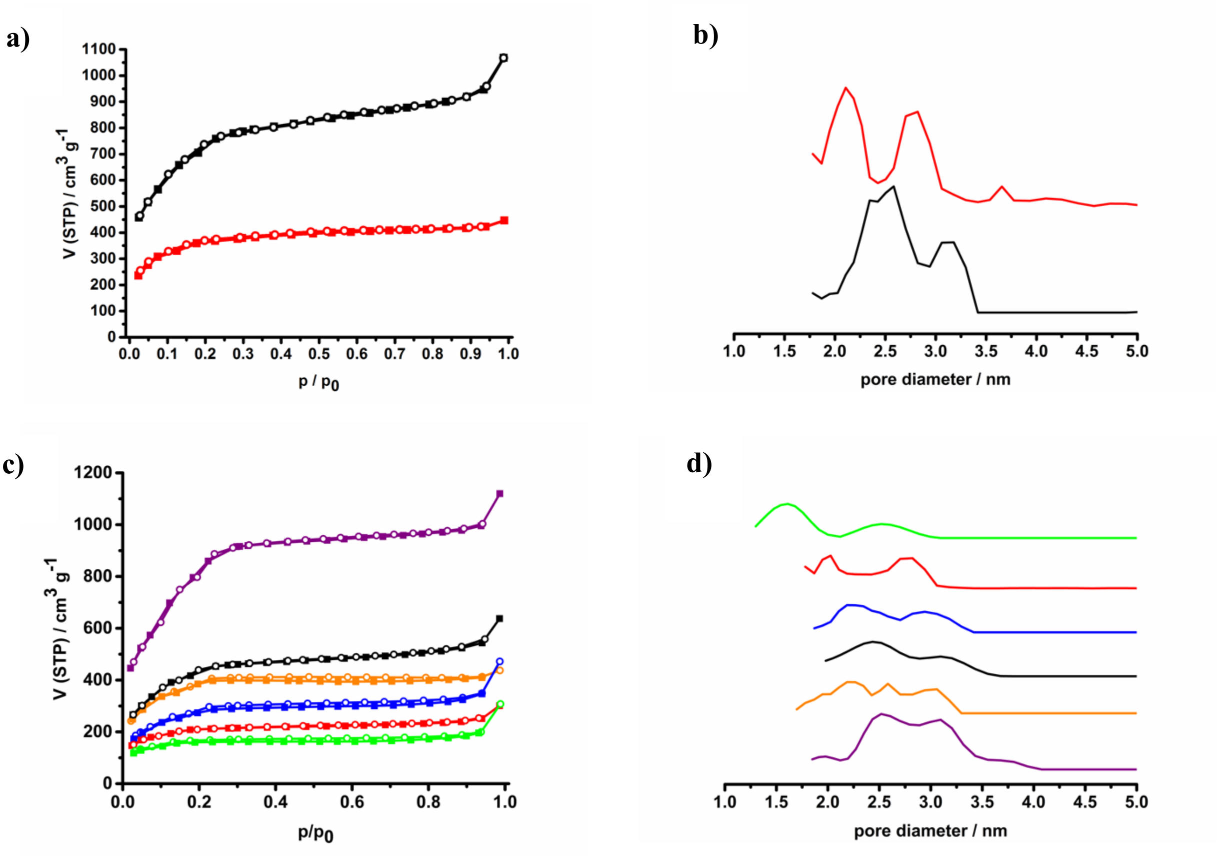

Figure S11: a) N_2 ad- (filled squares) and desorption (empty circles) isotherms at 77 K of Al-MIL-101-NH_2 (black curves) and Al-MIL-101-URPy (red curves); b) NLDFT pore size distribution curves of Al-MIL-101-NH_2 (black curve) and Al-MIL-101-URPy (red curve); c) N_2 ad- (full squares) and desorption isotherms at 77 K (empty circles) of H_2O-Cr-MIL-101-H (violet curves), DEA-Cr-MIL-101-H (orange curves), H_2O-Cr-MIL-101-NH_2 (black curves), DEA-Cr-MIL-101-NH_2 (blue curves), H_2O-Cr-MIL-101-URPy (red curves), DEA-Cr-MIL-101-URPy (green curves); d) NLDFT pore-size distribution curves H_2O-Cr-MIL-101-H (violet curve), DEA-Cr-MIL-101-H (orange curve), H_2O-Cr-MIL-101-NH_2 (black curve), DEA-Cr-MIL-101-NH_2 (blue curve), H_2O-Cr-MIL-101-URPy (red curve), DEA-Cr-MIL-101-URPy (green curve).

Table S2: Apparent BET-surface areas and total pore volumes determined at $p/p_0 = 0.95$ of the Al-MIl-101 Cr-MIL-101 derivatives.

	S_{BET} / $m^2\ g^{-1}$	$V_{total\ (p/p0\ =\ 0.95)}$ / $cm^3\ g^{-1}$
Al-MIL-101-NH$_2$	2345	1.29
Al-MIL-101-URPy	1325	0.65
H$_2$O-Cr-MIL-101-H	3011	1.54
DEA-Cr-MIL-101-H	1399	0.64
H$_2$O-Cr-MIL-101-NH$_2$	1615	0.84
DEA-Cr-MIL-101-NH$_2$	1096	0.54
H$_2$O-Cr-MIL-101-URPy	779	0.39
DEA-Cr-MIL-101-URPy	655	0.31

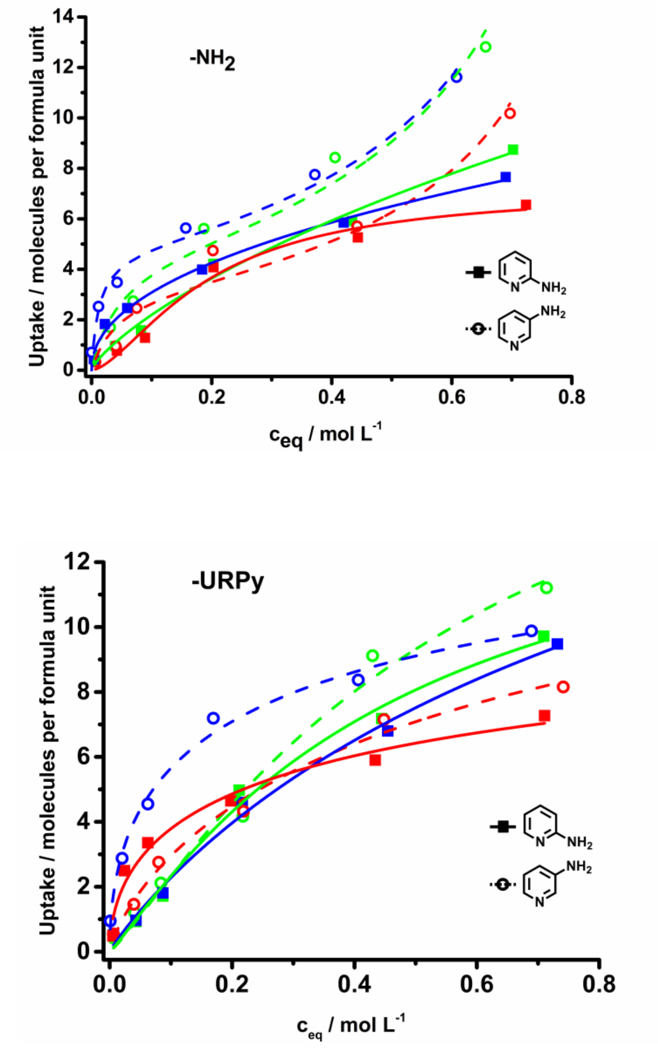

Figure S12: Single adsorption isotherms of 2-AP (solid squares) and 3-AP (empty circles) on a) H_2O-Cr-MIL-101-NH_2 (green curves), DEA-Cr-MIL-101-NH_2 (red curves) and Al-MIL-101-NH_2 (blue curves); b) H_2O-Cr-MIL-101-URPy (green curves), DEA-Cr-MIL-101-URPy (red curves) and Al-MIL-101-URPy (blue curves).

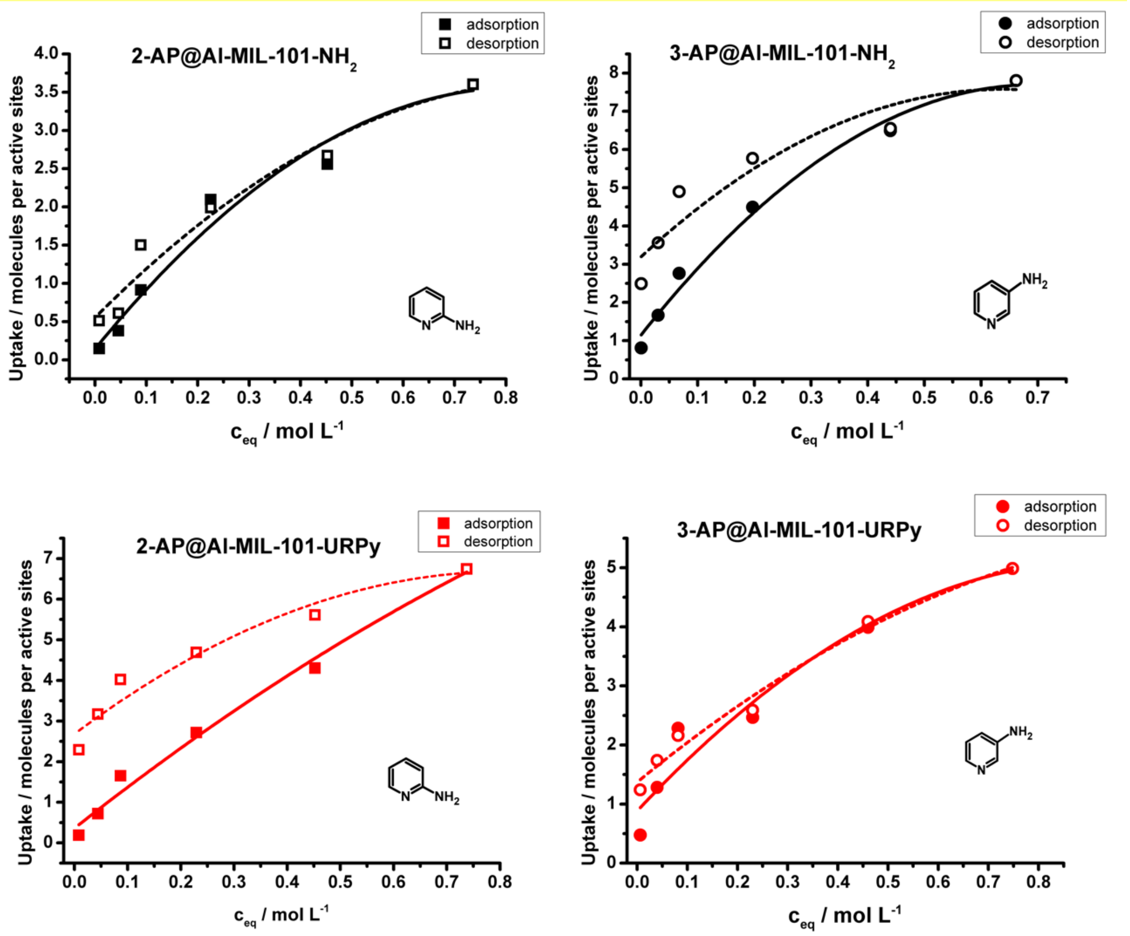

Figure S13: Comparison of adsorption and desorption isotherm for exposure of Al-MIL-101-NH$_2$ (black curves) and Al-MIL-101-URPy (red curves) to 2-AP (solid and open squares) and 3-AP (solid and open circles) solutions.

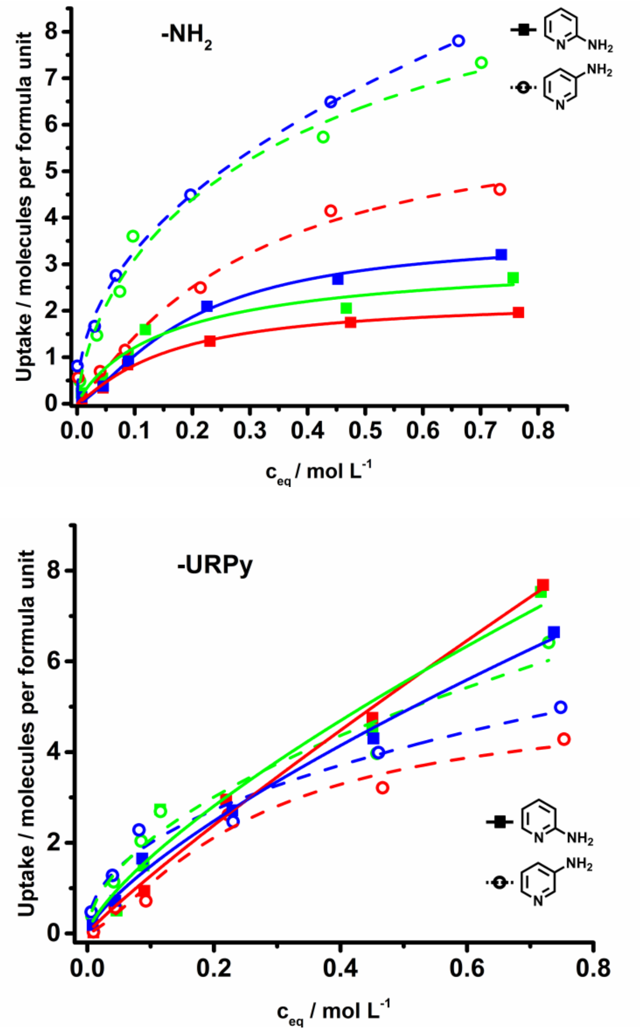

Figure S14: Competitive adsorption isotherms of 2-AP (solid squares) and 3-AP (empty circles) on a) H_2O@Cr-MIL-101-NH_2 (green curves), DEA@Cr-MIL-101-NH_2 (red curves) and Al-MIL-101-NH_2 (blue curves); and b) H_2O@Cr-MIL-101-URPy (green curves), DEA@Cr-MIL-101-URPy (red curves) and Al-MIL-101-URPy (blue curves).

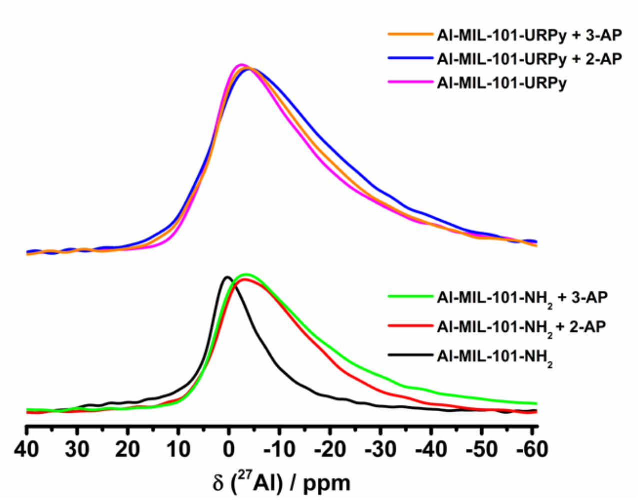

Figure S15: ^{27}Al NMR spectra of Al-MIL-101-NH$_2$ (black line), 2-AP@Al-MIL-101-NH$_2$ (red line), 3-AP@Al-MIL-101-NH$_2$ (green line), Al-MIL-101-URPy (magenta line), 2-AP@Al-MIL-101-URPy (blue line) and 3-AP@Al-MIL-101-URPy (orange line).

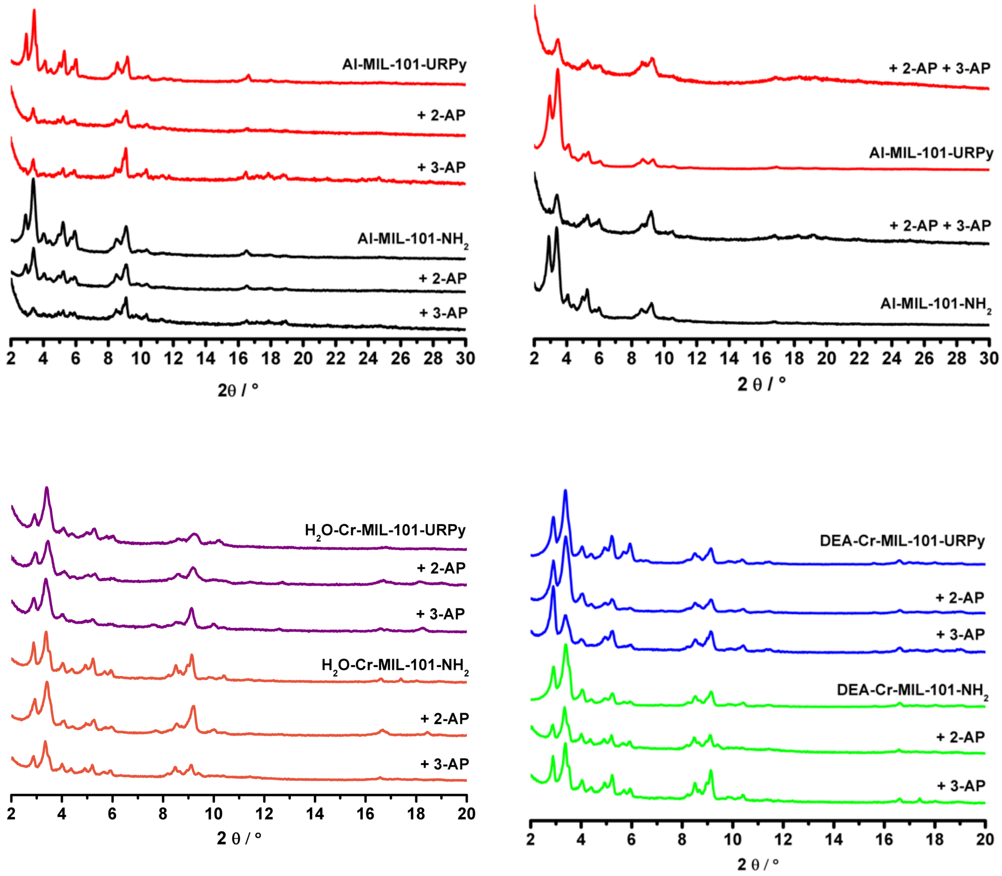

Figure S16: PXRD patterns of Al/Cr-MIL-101-X (X = NH$_2$ and URPy) loaded with 2-AP, 3-AP and mixtures thereof. From top left to down right: Al-MIL-101-X single adsorption of 2-AP and 3-AP, Al-MIL-101-X competitive adsorption of 2-AP and 3-AP, H$_2$O-Cr-MIL-101-X single adsorption of 2-AP and 3-AP and DEA-Cr-MIL-101-X single adsorption of 2-AP and 3-AP.

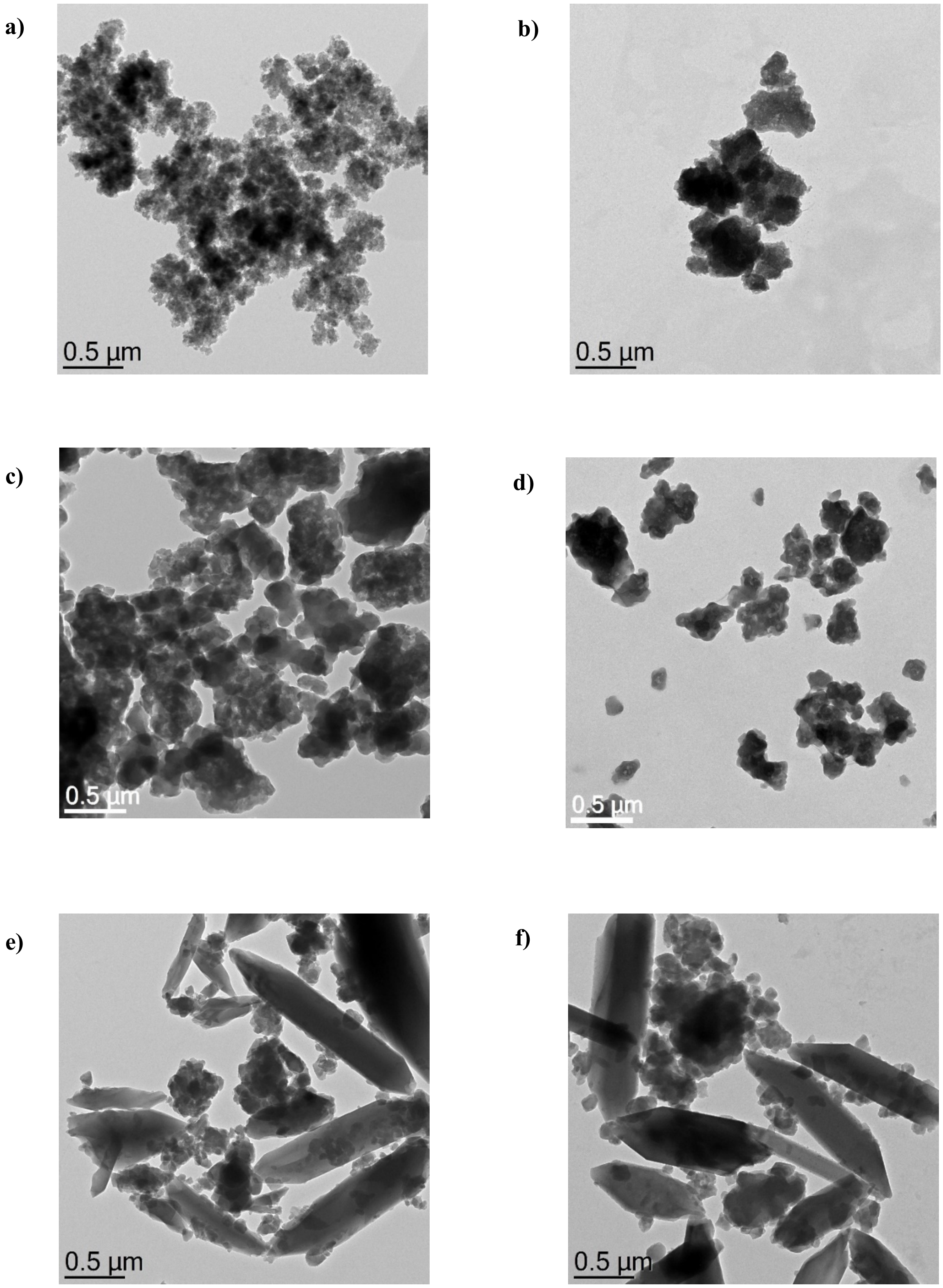

Figure S17: TEM images of a) Al-MIL-101-NH$_2$, b) Al-MIL-101-NH$_2$ loaded with 3 AP, c) Al-MIL-101-URPy, d) Al-MIL-101-URPy loaded with 3 AP, e) H$_2$O@Cr-MIL-101-NH$_2$, and f) H$_2$O@Cr-MIL-101-NH$_2$ loaded with 3 AP.

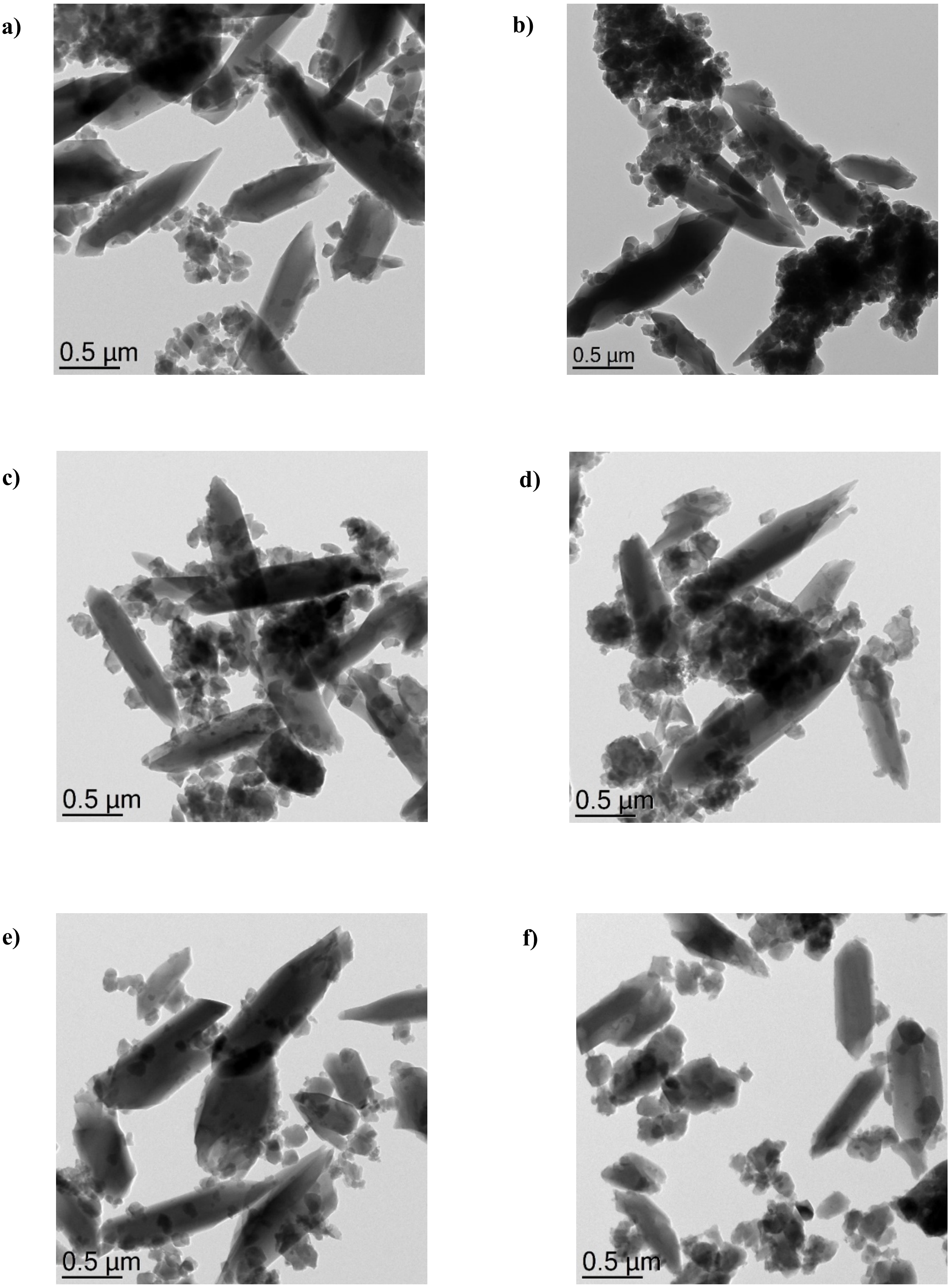

Figure S18: TEM images of a) H_2O@Cr-MIL-101-URPy, b) H_2O@Cr-MIL-101-URPy loaded with 3 AP, c) DEA@Cr-MIL-101-NH_2, d) DEA@Cr-MIL-101-NH_2 loaded with 3 AP, e) DEA@Cr-MIL-101-URPy, and f) DEA@Cr-MIL-101-URPy loaded with 3 AP.

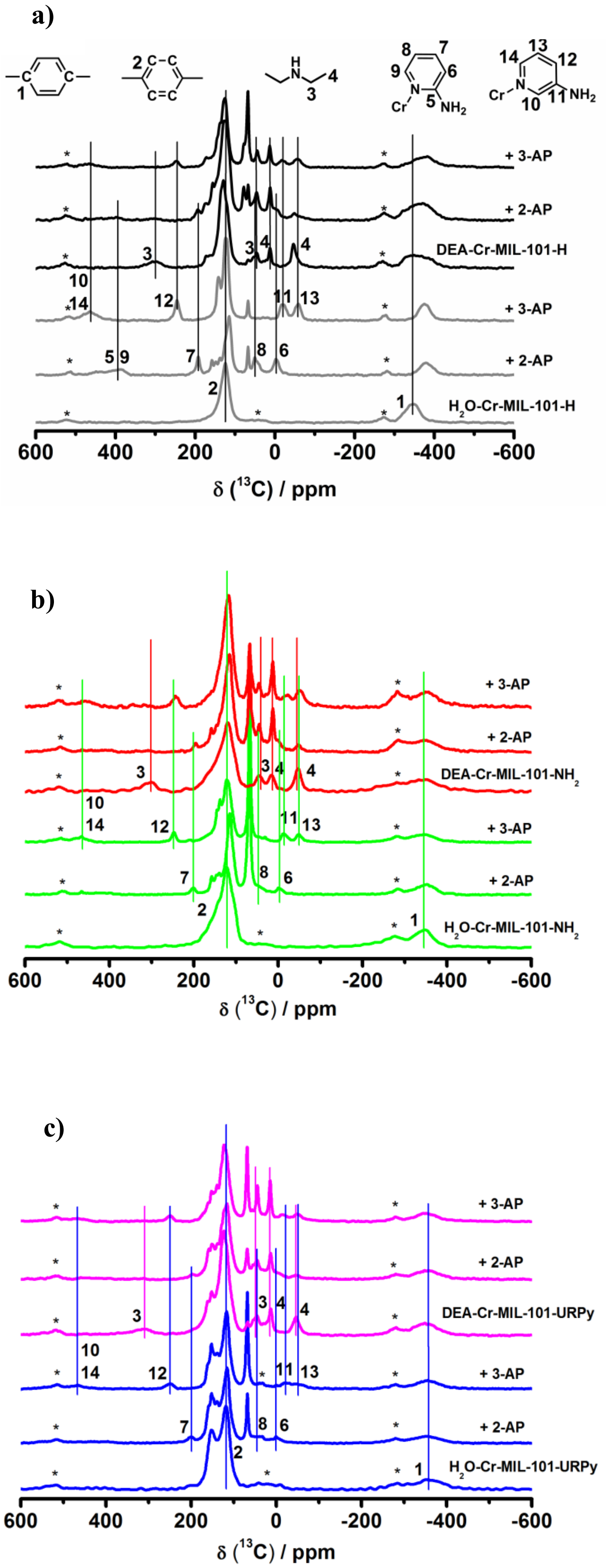

Figure S16: ^{13}C NMR spectra of 2-AP and 3-AP on a) H_2O/DEA-Cr-MIL-101-H, b) H_2O/DEA-Cr-MIL-101-NH_2 and c) H_2O/DEA-Cr-MIL-101-URPy.

Table S3: Comparison of experimental and calculated chemical shifts of Al-MIL-101-URPy, 2-AP@Al-MIL-101-URPy and 3-AP@Al-MIL-101-URPy. All shifts are given in ppm. The calculated shifts are given in color corresponding to the color code used for Figures 5 – 7.

	Assignment	N1	N2	N3	N4	N5
Al-MIL-101-URPy				-273.5	-262.4	-93.1
2-AP		-305.8	-124.2			
3-AP		-326.1	-72.0			
2-AP@Al-MIL-101-URPy	**0.05 M**	-298.4 / -308.9	-99.4 / -118.6	-272.9	-260.3	-99.4 / -118.6
	0.25 M	-300.2 / -309.5	-115.6 / -134.7	-272.3	-259.5	-115.6 / -134.7
	0.25 M / -25°C	-301.5	-119.9 / -134.7	-271.5	-258.9	-119.9 / -134.7
	DFT calculation	-298.5	-135.6	-272.7	-259.2	-111.8
3-AP@Al-MIL-101-URPy	**0.05 M**	-314.1 / -322.7	-77.0 / -97.7	-273.4	-261.0	-97.7 / -116.3
	0.25 M	-316.0 / -327.1	-78.3 / -99.0	-273.7	-260.8	-99.0 / -114.2
	0.25 M / -25°C	-315.7 / -323.8	-81.0 to -101.0	-272.3	-260.1	-96.8 / -114.8
	DFT calculation	-315.6	-94.3	-275.3	-254.9	-97.5
	DFT calculation	-324.3	-74.5	-272.8	-264.2	-114.5

References

1 T. Wittmann, A. Mondal, C. B. L. Tschense, J. J. Wittmann, O. Klimm, R. Siegel, B. Corzilius, B. Weber, M. Kaupp and J. Senker, *J. Am. Chem. Soc.*, 2018, **140**, 2135–2144.

2 Y. K. Hwang, D. Hong, J. Chang, S. H. Jhung, Y. Seo, J. Kim, A. Vimont, M. Daturi, C. Serre and G. Férey, *Angew. Chemie Int. Ed.*, 2008, **47**, 4144–4148.

3 M. Wickenheisser, F. Jeremias, S. K. Henninger and C. Janiak, *Inorganica Chim. Acta*, 2013, **407**, 145–152.

4 O. I. Lebedev, F. Millange, C. Serre, G. Van Tendeloo and G. Férey, *Chem. Mater.*, 2005, **17**, 6525–6527.

5 K. Krishnan and R. A. Plane, *Inorg. Chem.*, 1966, **5**, 852–857.

6 G. Socrates, *Infrared and Raman Characterisitc Group Frequencies. Tables and Charts*, JOHN WILEY & SONS LTD., Manchester, Third edit., 2001.